Structural investigation of the C-terminal catalytic fragment of presenilin 1

Solmaz Sobhanifar[a], Birgit Schneider[a], Frank Löhr[a], Daniel Gottstein[a], Teppei Ikeya[a], Krzysztof Mlynarczyk[b,c], Wojciech Pulawski[b], Umesh Ghoshdastider[b], Michal Kolinski[b], Slawomir Filipek[b,c], Peter Güntert[a,d], Frank Bernhard[a], and Volker Dötsch[a,1]

[a]Institute of Biophysical Chemistry and Center for Biomolecular Magnetic Resonance and Cluster of Excellence Macromolecular Complexes, Goethe University, 60438 Frankfurt/Main, Germany; [b]Laboratory of Biomodeling, International Institute of Molecular and Cell Biology, 02-109 Warsaw, Poland; [c]Faculty of Chemistry, University of Warsaw, 02-093 Warsaw, Poland; and [d]Frankfurt Institute for Advanced Studies, 60438 Frankfurt/Main, Germany

Edited by Peter E. Wright, The Scripps Research Institute, La Jolla, CA, and approved March 24, 2010 (received for review January 20, 2010)

The γ-secretase complex has a decisive role in the development of Alzheimer's disease, in that it cleaves a precursor to create the amyloid β peptide whose aggregates form the senile plaques encountered in the brains of patients. Γ-secretase is a member of the intramembrane-cleaving proteases which process their transmembrane substrates within the bilayer. Many of the mutations encountered in early onset familial Alzheimer's disease are linked to presenilin 1, the catalytic component of γ-secretase, whose active form requires its endoproteolytic cleavage into N-terminal and C-terminal fragments. Although there is general agreement regarding the topology of the N-terminal fragment, studies of the C-terminal fragment have yielded ambiguous and contradictory results that may be difficult to reconcile in the absence of structural information. Here we present the first structure of the C-terminal fragment of human presenilin 1, as obtained from NMR studies in SDS micelles. The structure reveals a topology where the membrane is likely traversed three times in accordance with the more generally accepted nine transmembrane domain model of presenilin 1, but contains unique structural features adapted to accommodate the unusual intramembrane catalysis. These include a putative half-membrane-spanning helix N-terminally harboring the catalytic aspartate, a severely kinked helical structure toward the C terminus as well as a soluble helix in the assumed-to-be unstructured N-terminal loop.

cell-free protein expression | gamma secretase | intramembrane proteolysis | membrane protein structure

Alzheimer's disease is the most common form of dementia and affects more than 25 million people worldwide. The most characteristic histological feature of Alzheimer's disease is the presence of long, insoluble amyloid fibrils composed of amyloid β (Aβ) peptide which, either alone or as reservoirs for soluble Aβ oligomers (1, 2), appear to be the primary species responsible for the massive neuronal injury presented in patients. Aβ generation is categorized under an unusual physiological phenomenon termed regulated intramembrane proteolysis. Here, the amyloid precursor protein first sheds its ectodomain mediated by β-secretase. The remaining membrane-bound C-terminal fragment is subsequently processed at a γ-cleavage site by the γ-secretase complex, a multisubunit protease whose minimal essential components include presenilin 1 (PS1) or presenilin-2 (PS2), anterior pharynx-defective, nicastrin, and presenilin enhancer 2 (3). The pathological relevance of this final step lies in the observation that γ-cleavage is variable and can occur after three distinct positions, 38, 40, and 42, whose selection influences the self-aggregating potential of the secreted Aβ peptide. Aβ42, although the minor species, appears to show the strongest potency for oligomerization and represents the majority of Aβ in amyloid plaques (4). Over 150 familial Alzheimer's disease associated mutations (www.molgen.ua.ac.be/ADMutations) have been linked to PS1, the catalytic subunit of the γ-secretase complex (5), the vast majority of which lead to an increase in the proportion of Aβ42 (6). Before activation, PS1 must undergo endoproteolysis, yielding natural N-terminal (NTF) and C-terminal (CTF) fragments, a process thought to cut and remove a loose helix that otherwise obstructs the substrate binding site in the immature enzyme (7). NTF and CTF harbor respective YD and GxGD conserved catalytic motifs, believed to contribute to a water-containing cavity in the γ-secretase complex wherein catalysis takes place (8, 9). CTF also contains a highly conserved PAL (proline, alanine, leucine) motif whose mutation leads to loss of PS activity (10, 11), and which has been suggested to contribute to the active-site conformation (12) and possibly to the formation of the water-containing pore (13). The sheer size and complexity of the γ-secretase complex has made its crystallographic investigation challenging, such that the analysis of the individual components may be a complementary approach. The NTF, in consensus with all published models, is believed to have a classical transmembrane topology consisting of six α-helices. In contrast, the models proposed for CTF topology vary greatly and are often irreconcilable (14–23). The most accepted PS1 model maintains a nine transmembrane segment (TMS) topology, three of which reside in CTF (14, 21, 22). The difficulty in obtaining a consensus model of CTF topology by biochemical methods nevertheless suggests an unorthodox structure. In light of evidence for the existence of a water-containing cavity required for catalysis, the more flexible micelle environment may be better suited for studying CTF than a solid membrane in the absence of other γ-secretase components necessary to constitute the hydrophilic pore. Here, CTF was studied by NMR spectroscopy in micelles, as well as by molecular modeling approaches.

Results

Prediction of Secondary Structure. One of the bottlenecks of structural investigation of the γ-secretase components is obtaining sufficient protein yields. Recently, we have shown that continuous-exchange cell-free expression is an interesting alternative to cell-based systems for the production of large quantities of membrane proteins (24, 25) and is particularly useful for isotope labeling in NMR samples (26). We and others have furthermore established that cell-free expressed membrane proteins can be functional when reconstituted into the correct detergent/lipid environment (27–29). CTF was produced by cell-free expression

Author contributions: F.B., S.F., and V.D. designed research; S.S., B.S., F.L., D.G., K.M., W.P., U.G., M.K., S.F., and P.G. performed research; S.S., B.S., F.L., D.G., T.I., K.M., W.P., U.G., M.K., S.F., P.G., F.B., and V.D. analyzed data; and S.S., S.F., and V.D. wrote the paper.

The authors declare no conflict of interest.

This article is a PNAS Direct Submission.

Data deposition: The NMR, atomic coordinates, chemical shifts, and restraints have been deposited in the Protein Data Bank, www.pdb.org (PDB ID code 2kr6) and the BioMagResBank, www.bmrb.wisc.edu (accession code 16625).

[1]To whom correspondence should be addressed. E-mail: vdoetsch@em.uni-frankfurt.de.

This article contains supporting information online at www.pnas.org/lookup/suppl/doi:10.1073/pnas.1000778107/-/DCSupplemental.

as a precipitate and solubilized in various detergents, of which SDS showed by far the most homogeneous behavior with a single Gaussian-shaped peak on the size-exclusion column and the best NMR spectroscopic characteristics (Fig. S1). To obtain backbone assignments, we used a combination of standard triple resonance experiments with uniform as well as TMS labeled samples (30), resulting in the assignment of 84% of the total resonances and 90% of resonances (E356-I467) excluding the N terminus which contains an unstructured loop. The combined chemical shift and NOE information revealed the presence of six α-helical regions (Fig. 1). The core of the protein consists of three helices of which, however, only the central helix 8 (T407-F428) shows typical transmembrane character. The preceding helix 7 (G384-A398) harbors the catalytic aspartate (D385) at its N terminus and appears too short to fully span the membrane. Although no helical secondary structure was found in the region R377-L383 preceding D385, this region harbors a classical GxxxG helix–helix interaction motif which may stabilize to form an interaction interface with substrates or other members of the γ-secretase complex. Furthermore, the sequence containing the conserved PAL motif (K430-T440) was not predicted as an α-helix and was found to be conformationally unstable, indicated by significant line broadening of resonances in this region. The C terminus of CTF contains a helical region stretching from F441 to A461 which, by the presence of a conserved proline (P455), is effectively divided into two shorter helices, helix 9a (F441-D450) and helix 9b (F456-A461). A short helix (helix α: M292-N297) containing the PS1 auto-cleavage site is in addition found at the very N terminus. Unexpectedly, we discovered another helix (helix β: E356-L369) in the assumed-to-be unstructured long N-terminal loop, whose amino acid composition is more typical of soluble helices.

Theoretical predictions (31, 32) agreed well with our experimentally determined topology for helix 8, but deviated slightly for helix 7 and strongly for helix 9b (Fig. 1). Both helices display weaker hydrophobic characteristics, suggesting they may not be standard transmembrane domains.

The topology of CTF was further investigated by [^{1}H, ^{15}N]-heteronuclear-NOE and amide hydrogen exchange experiments. Analysis of the heteronuclear-NOE experiments revealed negative and small positive NOEs typical of flexible and unstructured regions only for residues within the unstructured N-terminal loop, whereas the strongest positive enhancement was observed for residues within α-helical regions, including helix β (Fig. 1). Hydrogen-deuterium exchange studies showed that only amide hydrogens in helix 8 were still present after 26 h. Residues in helices 7 and 9 showed much faster deuterium exchange, suggesting they may be more exposed to the surrounding aqueous environment or may show greater dynamics (Fig. S2).

Determination of the Tertiary Structure. A major obstacle for the tertiary structure determination of α-helical membrane proteins is the limited availability of NOE-based long-range distance restraints. This is due to the increased size of the protein–micelle complex which necessitates the use of deuteration that eliminates most side-chain protons. Even without deuteration, however, the severe resonance overlap in the side-chain regions would make NOE assignment difficult. Consequently, most published NMR structures of α-helical membrane proteins are based on either few [DsbB (33), M2 (34)] or, in some cases, no [diacylglycerol

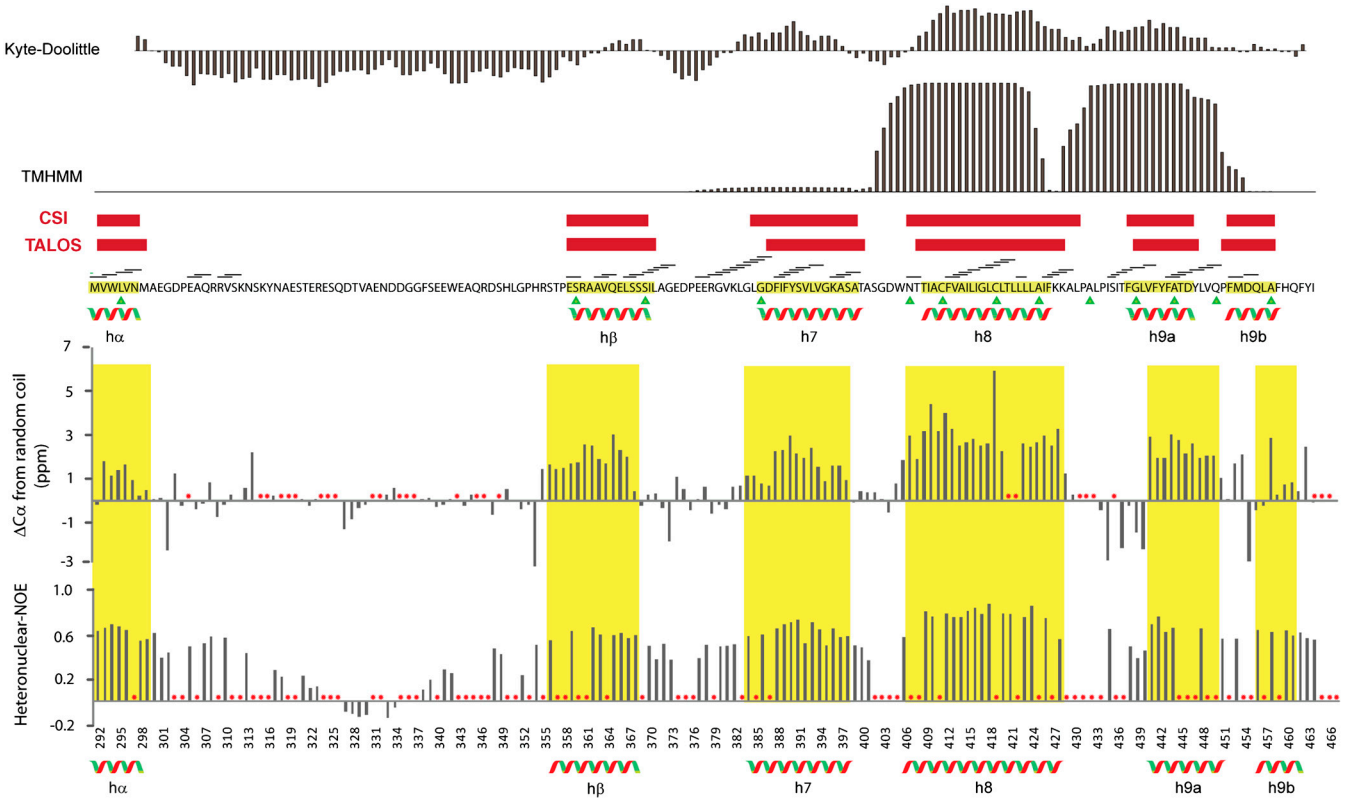

Fig. 1. Secondary structure prediction of CTF. The hydrophobicity plot was constructed with the Kyte-Doolittle algorithm, and transmembrane prediction using hidden Markov models (TMHMM) was used to predict for transmembrane segments. CSI (Chemical Shift Index) and TALOS (torsion angle likelihood obtained from shift and sequence similarity) were used to find secondary structure based on chemical shift data. Sequential NOEs observed in the ^{15}N-separated [^{1}H, ^{1}H]-NOESY spectrum are represented by bars above the sequence, and single cysteine mutation sites for PRE studies are shown by green triangles below the respective residues. The deviance of C$^\alpha$ residues from random coil, as well as the ^{15}N-heteronuclear-NOE are plotted against the sequence. Peaks that were overlapped, too weak, or missing for analysis are marked with red asterisks. Consensus α-helical regions are denoted in yellow as well as by α-helices below the sequence.

kinase (35)] long-range NOE restraints. To obtain long-range distance restraints, we employed paramagnetic relaxation enhancement (PRE) (36–39). Monocysteine mutants were obtained by mutating the two native cysteines of CTF to alanines [shown to have no effect on PS1 activity (40, 41)] and introducing a single cysteine at 13 different positions residing in both loops and helices (Fig. 1). Paramagnetic MTSL (methanethiosulfonate) labeled proteins were used to determine distances according to the method developed by Battiste and Wagner (39). Upper distance bounds of 12 Å and lower distance bounds of 20 Å were applied for peaks that were broadened beyond detection or unaffected by PRE, respectively, and those in between were assigned distances with a ±4 Å error margin. The resulting 168 upper- and 340 lower-bound distance restraints were combined with restraints for sequential NOEs, α-helical hydrogen bonds, and backbone torsion angles (Fig. S3 *A* and *B* and Table S1). The structure calculated with CYANA (42) consisted of six α-helical elements (Fig. 2 and Table S1). Helix 8 is the only segment long enough to fully traverse a lipid bilayer and is mildly kinked at the highly conserved G417 position whose mutation leads to loss of function (13). Helix 7 is shorter than expected for a membrane-spanning helix, and its N-terminal active-site D385 is positioned at what would be the center of the bilayer where cleavage is proposed to occur. Helix 9 assumes an unusual conformation in that it contains a dominant kink at the highly conserved P455 position, effectively dividing it into helices 9a and 9b. Helix 9a lies approximately perpendicular to helices 7 and 8, suggesting it to be embedded roughly horizontally below what would be the surface of the membrane, whereas helix 9b points toward the surface of the membrane. Helix β within the N-terminal loop was found near the core of the protein, although not tightly connected to it. Lastly, no significant contacts were found between the short N-terminal helix α and the other α-helical elements.

Probing of Surface Accessibility and Cross-Validation with Existing Biochemical Data. The structural characterization described here was performed on CTF in isolation. Structural validation via functional analysis would require not only the NTF, but all four components of the γ-secretase which, even if properly reconstituted, would make NMR investigation unfeasible. Here we cross-validated our structure against biochemical surface accessibility mapping data obtained by others in the context of the active complex (13, 40, 41, 43). The surface accessibility of CTF was probed by performing 3D Transverse Relaxation Optimized Spectroscopy (TROSY)-HNCA measurements (to overcome peak overlap) in the presence of either Mn^{2+}, 5-doxyl stearic acid (5-DSA), or 16-doxyl stearic acid (16-DSA), all of which induce line-broadening in nearby residues (Fig. 3*A*). The free Mn^{2+} results in the broadening of surface-exposed residues. Due to the negatively charged SDS head group, the Mn^{2+} ions appear to cluster and likely form a shell around the SDS micelle, such that amino acids further away from the micelle may experience a lesser degree of broadening than those closer to the micellar surface. The 5-DSA and 16-DSA, whose tails bury inside the micelle and whose paramagnetic doxyl groups reside within the upper and lower regions of the micelle respectively, should broaden residues either at the solvent–micelle interface or embedded within the micelle. Residues unaffected by all three broadening reagents would be expected to be fully solvent exposed and remote from the micellar surface. CTF contains a predicted long N-terminal loop whose central region is not significantly broadened by any of the paramagnetic reagents, suggesting its remote location from the micelle. However, helix α as well as nearby residues (R308-N312) seem to be either embedded or in close proximity to the micelle. Furthermore, helix β was moderately broadened by all three paramagnetic reagents, suggesting it lies close to the surface of the micelle. Similarly, the highly conserved PAL motif was broadened to some extent by all reagents, such that it likely lies outside of, but remains associated with the micelle. The central region of helix 7 appears to be embedded within the micelle (5-DSA and 16-DSA strongly broaden K387-D389) and highly associated with the micelle in flanking regions. Most residues in helix 8 as well as those in helix 9a disappear almost entirely in the presence of 5-DSA or 16-DSA, implying they are micelle embedded. In addition, residues in helix 9b show moderate broadening by all three reagents, suggesting a micelle associated rather than embedded location. These results were supported by analysis of the 3D ^{15}N-separated [^{1}H, ^{1}H]-NOESY spectrum for water-exchange signals of exposed residues, as well as for NOEs between SDS and residues in close proximity to the detergent (Fig. 3*B* and Fig. S4). We next compared our surface accessibility data to those of several groups who recently employed substituted cysteine accessibility to probe structural features of CTF in the context of the entire membrane-embedded γ-secretase complex (Fig. 3*C* and Table S2). Sato et al. (40) and Tolia et al. (41) showed that several positions in helix 7, including the catalytic D385 (41), are surface-accessible, consistent with the presence of a water-filled cavity, whereas the central region of helix 7 is membrane-embedded. Both groups in addition observed that all residues in helix 9 were to some extent accessible to the surface, although many in helix 9a showed restricted reactivities, and furthermore postulated that helices 9a and 9b, connected by a proline kink, have different orientations (13, 43). In accordance, our surface accessibility data showed that helix 7 is partly micelle embedded, whereas the region N-terminal to the GxGD catalytic motif is surface accessible and close to the

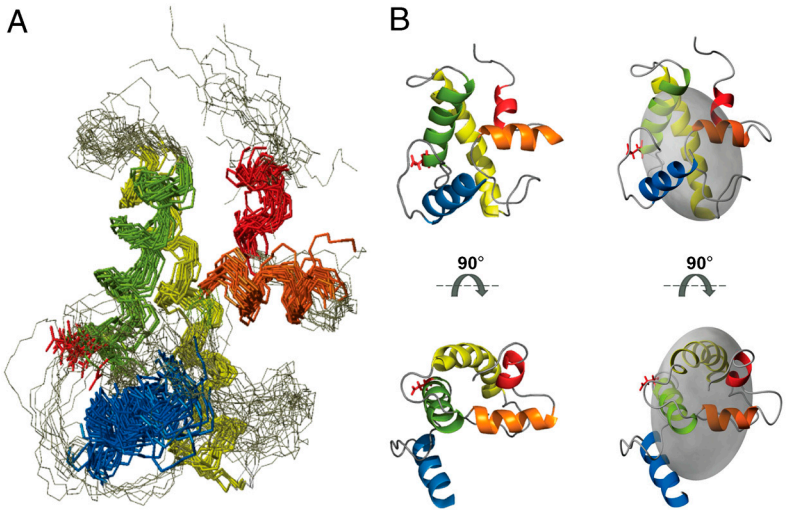

Fig. 2. CTF structure. (*A*) Bundle diagram of the 20 lowest energy CYANA conformers representing the final NMR structure, obtained by superpositioning the backbone atoms of residues E356-L369, L384-A398, I407-F428, F441-T450, and F456-A461. (*B*) Ribbon diagram of the lowest energy conformer in two different orientations (*Left*) and its placement within a symmetric shell representing the potential relative position of the micelle (*Right*). Color scheme: helix β in blue, helix 7 in green, helix 8 in yellow, helix 9a in orange, helix 9b in red, and D385 displayed as ball and stick in red. Structures are shown without the long N-terminal loop for simplicity.

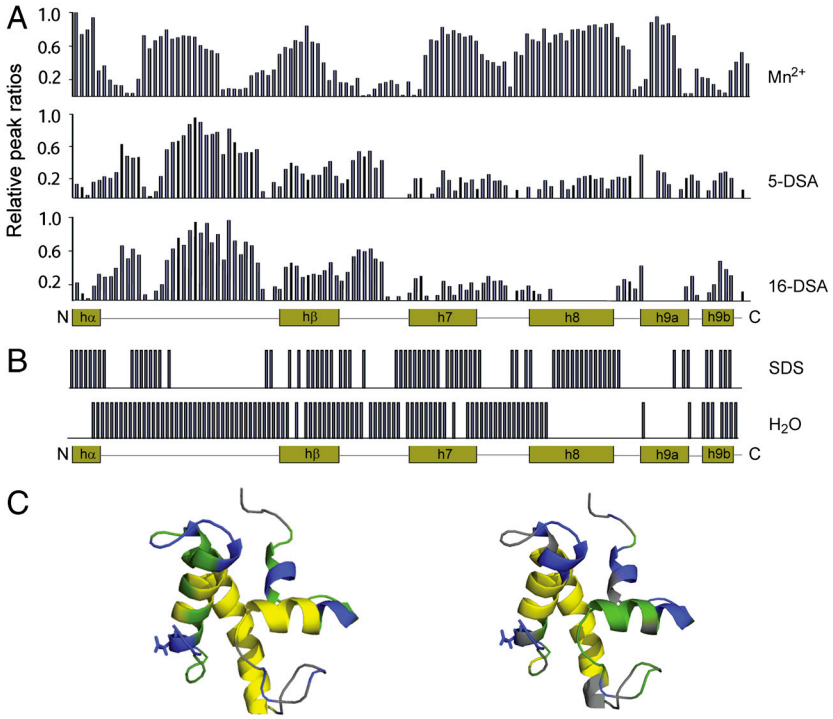

Fig. 3. Surface accessibility of CTF. (*A*) The effect of paramagnetic broadening reagents on residues are displayed as peak-height ratios of resonances, determined in the presence and absence of 0.2 mM Mn^{2+}, 3.0 mM 5-DSA, or 3.0 mM 16-DSA. Residue broadening by Mn^{2+} or 5/16-DSA indicates surface accessibility or micelle insertion, respectively. Residues broadened by both Mn^{2+} and 5/16-DSA lie at the solvent–micelle interface, whereas those broadened by neither are remote from the micellar surface. The green bars beneath indicate the location of the predicted α-helical structural elements. (*B*) The presence or absence of water-exchange peaks and intermolecular NOE cross-peaks to the methylene groups of SDS are indicated, as obtained from the ^{15}N-separated [^{1}H, ^{1}H]-NOESY spectrum. Four patterns were observed with residues showing exclusive water-exchange signals (water-exposed), exclusive cross-peaks to SDS resonances (micelle-embedded), as well as both (micelle-associated) or neither (weak signal). In *A* and *B*, residues with too weak and/or overlapped signals were excluded from the analysis. (*C*) Comparison of surface accessibility from our studies (*Left*) and those of others via cysteine scanning analyses (*Right*). Accessible (blue), partially accessible (green), and nonaccessible (yellow) regions were mapped onto our ribbon diagram of CTF. Residues for which data were unavailable or ambiguous due to conflicting results are shown in gray. D385 is displayed in ball and stick format. Structures are shown without the long N-terminal loop and helix β for simplicity.

micelle. Our data also showed that helix 9 is severely kinked and indeed assumes a unique conformation. Although residues in helix 9b are surface-accessible, those in helix 9a showed little or no such accessibility. Furthermore, several residues at the extreme C terminus including the last residue of helix 9b (A461-H463) showed close contacts to the micelle as indicated by their paramagnetic broadening patterns as well as cross-peaks to SDS. The surface accessibility of the last three C-terminal residues (F465-I467) could not be assessed due to lack of assignment. Finally, both Sato et al. and Tolia et al. showed that residues in helix 8 are buried within the membrane (13, 43), which agrees well with our findings.

Molecular Dynamics Simulations Within Detergent and Lipid Bilayer Environments. To further evaluate our structure of CTF, we performed molecular dynamics simulation in micelles and in lipid bilayers. To achieve a sufficient simulation time needed for micelle formation and extensive sampling of conformational space, we chose a coarse-grain approach using MARTINI, primarily developed to study the behavior of biological membrane systems (44, 45). Simulations were carried out with 200 coarse-grain dodecylphosphocholine (DPC) molecules which formed a micelle consisting of about 80 molecules around CTF during the first 50 ns, during which time the structure of CTF was frozen. In the ensuing 3 μs simulation, the coarse-grain structure of CTF was allowed to change. Comparison with the initial NMR structure revealed that the interhelical angle between helices 7 and 8 remained relatively stable (140° in the NMR structure and 120° after the 3 μs simulation) and helices 9a and 9b became more antiparallel (105° in the NMR structure and 130° after simulation) (Fig. 4 and Fig. S5*A*).

We also carried out coarse-grain simulations in dilauroylphosphatidylcholine (DLPC) and dipalmitoylphosphatidylcholine (DPPC) bilayers with MARTINI (Fig. S5*B*) as well as molecular dynamics simulations of an all-atom representation of CTF employing continuous environments with the Implicit Membrane Model (46) in CHARMM (47) (Fig. S5*C*). The resulting structures showed larger differences both with respect to the NMR input structure as well as to each other. Although the angle between helices 7 and 8 remained relatively stable, that between helices 9a and 9b changed depending on the thickness of the membrane. In addition, the position of the catalytic helix also shifted from the center of the membrane toward its border, again depending on membrane width. These results again would suggest that the micelle is a better environment for the isolated CTF than a solid bilayer given that certain of its elements are believed to reside in close proximity to the water-filled cavity existing within the γ-secretase complex.

Discussion

In our study, we present the solution-state NMR structure of CTF in SDS micelles. An important question to ask is how well the structure obtained in the context of a surrogate environment such as the SDS micelle would approximate the natural conformation within the lipid bilayer. Although SDS is generally recognized to

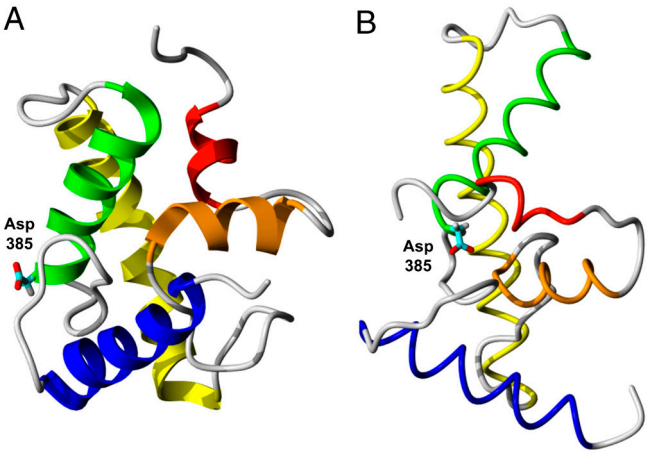

Fig. 4. Comparison of CTF NMR and molecular dynamics (MD) simulated structures. (*A*) Ribbon diagram of the lowest energy conformer from NMR investigation. (*B*) C^{α} trace after 3 μs of coarse-grain MD simulation in a DPC detergent/water mixture. Color scheme: helix β in blue, helix 7 in green, helix 8 in yellow, helix 9a in orange, and helix 9b in red. D385 is displayed in ball and stick format. Structures are shown without the long N-terminal loop for simplicity.

denature water-soluble proteins, hydrophobic regions of integral membrane proteins have been shown to display a strong affinity in their native state for complete detergent micelles (48–51). Indeed, structures of several integral membrane proteins such as the tetrameric KcsA potassium channel (52), the Na,K-ATPase regulatory protein FXYD1 (53), MerF of the bacterial mercury detoxification system (54), and subunit c of ATP synthase (55) have been investigated in SDS by NMR spectroscopy. Nevertheless, given the fact that CTF was studied in isolation in the absence of the other γ-secretase components and outside of its natural bilayer environment, it is imperative to validate our structure by comparing it to surface accessibility studies performed by several groups on the native PS1. Early topological reports were based on gene fusion studies in which truncated versions of PS1 were fused to reporter proteins that could be modified according to their cytoplasmic or extracytoplasmic locations. These studies yielded six (18), seven (17), and eight (15, 56) TMS models of PS1, where CTF was predicted to contain from zero to two transmembrane helices. This inconsistency owes likely to the approach, which may suffer from artifacts related to truncation and the nature of reporter proteins. Less intrusive approaches for studying the intact PS1 include the use of small glycosylation acceptor sequences or antibody-based immunofluorescence. With the first approach, several studies provided evidence in support of a nine TMS topology, where helices 7, 8, and 9 traverse the membrane (14, 21, 22). Dewji et al. (16, 23) using immunofluorescence, however, proposed a seven TMS model where only helix 8 of CTF traverses the membrane (however, their results which predict one TMS in CTF are also consistent with a three TMS topology). The proposed topologies above are summarized in Fig. S6. Our structure suggests that CTF traverses the membrane three times, although several unusual features are observed, such as the putative half-membrane-spanning helix 7 as well as the kinked helix 9. Recently, single particle electron microscopy has revealed the presence of a large 20–40 Å interior chamber within the active purified γ-secretase complex (8, 9). X-ray crystallographic analyses of site-2 protease (57) and rhomboid (58), both members of the intramembrane-cleaving proteases, have further shown the presence of active sites in water-filled cavities within the bilayer. It is thus likely that elements of the CTF are partly exposed to a hydrophilic pore, which would be consistent with our surface accessibility analysis. Furthermore, our hydrogen exchange measurements showed relatively fast exchange in regions outside of helix 8 implying either higher exposure to the aqueous environment and/or increased dynamics.

Cross-validation of our surface accessibility studies with those performed by others on CTF in the context of the active γ-secretase complex revealed many similarities. A minor discrepancy was nevertheless observed in helix 9a, which we found to have little to no access to the surface, but which others found to have weak and/or restricted exposure (13, 43). This might be explained with differences in the depth at which helix 9a is located in a bilayer versus a micelle. Furthermore, Sato et al. (13) and Tolia et al. (43) both reported that the PAL motif and the active-site residues in helix 6 of NTF are in close proximity (~5 Å) based on cross-linking experiments, although Tolia et al. (43) were unable to cross-link the PAL region to the catalytic D385 in helix 7. Our structure positions the PAL region away from the catalytic GxGD motif. An explanation could be that the PAL loop changes conformation in the active complex, positioning it close to the active site.

We also compared CTF to the crystal structure of the rhomboid protease (58) where the catalytic serine on helix S4 is located near the center of the membrane. Similarly, helix 7 of CTF which contains the catalytic D385 appears to only traverse the membrane partly. The other curious feature of rhomboid is the presence of the membrane-embedded α-helix-containing loop, which is inserted below the surface of the lipid bilayer and contains a prominent kink, reminiscent of helix 9 in CTF. Although the conformation of CTF as observed in micelles may possibly change due to interaction with other components in the context of the entire multisubunit γ-secretase complex, the similarity of the above-mentioned features with those of the rhomboid, as well as their cross-validation with surface accessibility experiments performed in the context of the entire γ-secretase, suggest that the core α-helical elements are likely preserved in the active complex. It may therefore be possible that proteins involved in intramembrane proteolysis share similar structural features adapted to their unique function.

An unanticipated soluble but membrane-associated α-helix (helix β) was observed within the long N-terminal loop of CTF, which up until now was thought to be without structure. Interestingly, a study of the familial Alzheimer's disease mutational patterns encountered in patients (www.molgen.ua.ac.be/ADMutations) revealed that several mutation sites were located in and around helix β, yet only one was found in the long and poorly conserved N-terminal loop, suggesting that helix β could play a functional role. Familial Alzheimer's disease mutational patterns in addition revealed that although several sites were found in helices 7 and 8, none were encountered in helix 9. Given that familial Alzheimer's disease mutations most often lead to an increase in the ratio of Aβ42 to Aβ40, the lack of mutation sites within helix 9 may suggest that it is not directly involved in the cut site selection process.

Materials and Methods

CTF-PS1 was cloned into a modified pET21a vector and expressed in a S30-based continuous-exchange cell-free system. Proteins were stable-isotope labeled by addition of the labeled amino acids directly to the reaction mixture, and were expressed as a precipitate and solubilized in 100 mM ultrapure SDS in the presence of 20 mM BisTrisPropane (pH 6.8) and 20 mM KCl. Purification steps were not required due to the sufficient purity of the solubilized protein. The homogeneity of the samples was analyzed by size-exclusion chromatography. TROSY-type HNCA, HN(CO)CA, HNCACB, HNCACO, HNCO, and ^{15}N-separated [^{1}H, ^{1}H]-NOESY measurements were acquired for backbone assignment. PRE experiments for collection of long-range distance restraints were performed using MTSL labeled monocysteine mutants. Surface accessibility analyses were carried out by addition of water-soluble Mn^{2+} or membrane-targeted 5-DSA and 16-DSA paramagnetic reagents to the solubilized protein, followed by TROSY-HNCA measurements. Spectra were analyzed with CARA (www.nmr.ch) and Sparky (T. D. Goddard and D. G Kneller, University of California, San Francisco). Structure calculations were performed using CYANA (42). Coarse-grain molecular dynamics simulations were carried out with Gromacs (59, 60) for simulations in DPC micelles and in DPPC and DLPC bilayers. Simulations in continuous environments were performed using CHARMM (47). Images were constructed with MOLMOL (61) and PYMOL (www.pymol.org). Further details are provided in SI Text.

ACKNOWLEDGMENTS. This work was supported by the Center for Biomolecular Magnetic Resonance at the University Frankfurt, the Deutsche Forschungsgemeinschaft (Sonderforschungsbereich 807), the Center for Membrane Proteomics, and the Cluster of Excellence Frankfurt (Macromolecular Complexes). P.G. acknowledges support by the Lichtenberg program of the Volkswagen Foundation. The research leading to these results has received funding from the European Community's Seventh Framework Program [(FP7/2007-2013) under grant agreement 211800 and from EU-Grant European Drug Initiative on Channels and Transporters (Health F4-2007-201924)].

1. Dahlgren KN, et al. (2002) Oligomeric and fibrillar species of amyloid-beta peptides differentially affect neuronal viability. *J Biol Chem* 277:32046–32053.
2. Tomic JL, Pensalfini A, Head E, Glabe CG (2009) Soluble fibrillar oligomer levels are elevated in Alzheimer's disease brain and correlate with cognitive dysfunction. *Neurobiol Dis* 35:352–358.
3. Sato T, et al. (2007) Active gamma-secretase complexes contain only one of each component. *J Biol Chem* 282:33985–33993.
4. Roher AE, et al. (1993) beta-Amyloid-(1-42) is a major component of cerebrovascular amyloid deposits: implications for the pathology of Alzheimer disease. *Proc Natl Acad Sci USA* 90:10836–10840.

5. Wolfe MS, et al. (1999) Two transmembrane aspartates in presenilin-1 required for presenilin endoproteolysis and gamma-secretase activity. *Nature* 398:513–517.
6. Tanzi RE, Bertram L (2005) Twenty years of the Alzheimer's disease amyloid hypothesis: A genetic perspective. *Cell* 120:545–555.
7. Knappenberger KS, et al. (2004) Mechanism of gamma-secretase cleavage activation: Is gamma-secretase regulated through autoinhibition involving the presenilin-1 exon 9 loop?. *Biochemistry* 43:6208–6218.
8. Lazarov VK, et al. (2006) Electron microscopic structure of purified, active gamma-secretase reveals an aqueous intramembrane chamber and two pores. *Proc Natl Acad Sci USA* 103:6889–6894.
9. Osenkowski P, et al. (2009) Cryoelectron microscopy structure of purified gamma-secretase at 12 A resolution. *J Mol Biol* 385:642–652.
10. Kaether C, et al. (2004) The presenilin C-terminus is required for ER-retention, nicastrin-binding and gamma-secretase activity. *EMBO J* 23:4738–4748.
11. Wang J, Brunkan AL, Hecimovic S, Walker E, Goate A (2004) Conserved "PAL" sequence in presenilins is essential for gamma-secretase activity, but not required for formation or stabilization of gamma-secretase complexes. *Neurobiol Dis* 15:654–666.
12. Wang J, et al. (2006) C-terminal PAL motif of presenilin and presenilin homologues required for normal active site conformation. *J Neurochem* 96:218–227.
13. Sato C, Takagi S, Tomita T, Iwatsubo T (2008) The C-terminal PAL motif and transmembrane domain 9 of presenilin 1 are involved in the formation of the catalytic pore of the gamma-secretase. *J Neurosci* 28:6264–6271.
14. Oh YS, Turner RJ (2005) Topology of the C-terminal fragment of human presenilin 1. *Biochemistry* 44:11821–11828.
15. Li X, Greenwald I (1998) Additional evidence for an eight-transmembrane-domain topology for Caenorhabditis elegans and human presenilins. *Proc Natl Acad Sci USA* 95:7109–7114.
16. Dewji NN, Valdez D, Singer SJ (2004) The presenilins turned inside out: Implications for their structures and functions. *Proc Natl Acad Sci USA* 101:1057–1062.
17. Nakai T, et al. (1999) Membrane topology of Alzheimer's disease-related presenilin 1. Evidence for the existence of a molecular species with a seven membrane-spanning and one membrane-embedded structure. *J Biol Chem* 274:23647–23658.
18. Lehmann S, Chiesa R, Harris DA (1997) Evidence for a six-transmembrane domain structure of presenilin 1. *J Biol Chem* 272:12047–12051.
19. Henricson A, Kall L, Sonnhammer EL (2005) A novel transmembrane topology of presenilin based on reconciling experimental and computational evidence. *FEBS J* 272:2727–2733.
20. Doan A, et al. (1996) Protein topology of presenilin 1. *Neuron* 17:1023–1030.
21. Spasic D, et al. (2006) Presenilin-1 maintains a nine-transmembrane topology throughout the secretory pathway. *J Biol Chem* 281:26569–26577.
22. Laudon H, et al. (2005) A nine-transmembrane domain topology for presenilin 1. *J Biol Chem* 280:35352–35360.
23. Dewji NN, Singer SJ (1997) The seven-transmembrane spanning topography of the Alzheimer disease-related presenilin proteins in the plasma membranes of cultured cells. *Proc Natl Acad Sci USA* 94:14025–14030.
24. Klammt C, Schwarz D, Dotsch V, Bernhard F (2007) Cell-free production of integral membrane proteins on a preparative scale. *Method Mol Biol* 375:57–78.
25. Schwarz D, et al. (2007) Preparative scale expression of membrane proteins in Escherichia coli-based continuous exchange cell-free systems. *Nat Protoc* 2:2945–2957.
26. Sobhanifar S, et al. (2010) Cell-free expression and stable isotope labelling strategies for membrane proteins. *J Biomol NMR* 46:33–43.
27. Chen YJ, et al. (2007) X-ray structure of EmrE supports dual topology model. *Proc Natl Acad Sci USA* 104:18999–19004.
28. Keller T, et al. (2008) Cell free expression and functional reconstitution of eukaryotic drug transporters. *Biochemistry* 47:4552–4564.
29. Klammt C, et al. (2005) Evaluation of detergents for the soluble expression of alpha-helical and beta-barrel-type integral membrane proteins by a preparative scale individual cell-free expression system. *FEBS J* 272:6024–6038.
30. Reckel S, et al. (2008) Transmembrane segment enhanced labeling as a tool for the backbone assignment of alpha-helical membrane proteins. *Proc Natl Acad Sci USA* 105:8262–8267.
31. Kyte J, Doolittle RF (1982) A simple method for displaying the hydropathic character of a protein. *J Mol Biol* 157:105–132.
32. Krogh A, Larsson B, von Heijne G, Sonnhammer EL (2001) Predicting transmembrane protein topology with a hidden Markov model: Application to complete genomes. *J Mol Biol* 305:567–580.
33. Zhou Y, et al. (2008) NMR solution structure of the integral membrane enzyme DsbB: Functional insights into DsbB-catalyzed disulfide bond formation. *Mol Cell* 31:896–908.
34. Schnell JR, Chou JJ (2008) Structure and mechanism of the M2 proton channel of influenza A virus. *Nature* 451:591–595.
35. Van Horn WD, et al. (2009) Solution nuclear magnetic resonance structure of membrane-integral diacylglycerol kinase. *Science* 324:1726–1729.
36. Krueger-Koplin RD, et al. (2004) An evaluation of detergents for NMR structural studies of membrane proteins. *J Biomol NMR* 28:43–57.
37. Liang B, Bushweller JH, Tamm LK (2006) Site-directed parallel spin-labeling and paramagnetic relaxation enhancement in structure determination of membrane proteins by solution NMR spectroscopy. *J Am Chem Soc* 128:4389–4397.
38. Roosild TP, et al. (2005) NMR structure of Mistic, a membrane-integrating protein for membrane protein expression. *Science* 307:1317–1321.
39. Battiste JL, Wagner G (2000) Utilization of site-directed spin labeling and high-resolution heteronuclear nuclear magnetic resonance for global fold determination of large proteins with limited nuclear overhauser effect data. *Biochemistry* 39:5355–5365.
40. Sato C, Morohashi Y, Tomita T, Iwatsubo T (2006) Structure of the catalytic pore of gamma-secretase probed by the accessibility of substituted cysteines. *J Neurosci* 26:12081–12088.
41. Tolia A, Chavez-Gutierrez L, De Strooper B (2006) Contribution of presenilin transmembrane domains 6 and 7 to a water-containing cavity in the gamma-secretase complex. *J Biol Chem* 281:27633–27642.
42. Güntert P (2004) Automated NMR structure calculation with CYANA. *Method Mol Biol* 278:353–378.
43. Tolia A, Horre K, De Strooper B (2008) Transmembrane domain 9 of presenilin determines the dynamic conformation of the catalytic site of gamma-secretase. *J Biol Chem* 283:19793–19803.
44. Bond PJ, Sansom MS (2006) Insertion and assembly of membrane proteins via simulation. *J Am Chem Soc* 128:2697–2704.
45. Marrink SJ, Risselada HJ, Yefimov S, Tieleman DP, de Vries AH (2007) The MARTINI force field: Coarse grained model for biomolecular simulations. *J Phys Chem B* 111:7812–7824.
46. Lazaridis T (2003) Effective energy function for proteins in lipid membranes. *Proteins* 52:176–192.
47. Brooks B, et al. (1983) CHARMM: A program for macromolecular energy, minimization, and dynamics calculations. *J Comput Chem* 4:187–217.
48. Tanford C, Reynolds JA (1976) Characterization of membrane proteins in detergent solutions. *Biochim Biophys Acta* 457:133–170.
49. Fisher LE, Engelman DM, Sturgis JN (2003) Effect of detergents on the association of the glycophorin a transmembrane helix. *Biophys J* 85:3097–3105.
50. Thevenin D, Lazarova T (2008) Stable interactions between the transmembrane domains of the adenosine A2A receptor. *Protein Sci* 17:1188–1199.
51. Zhou FX, Cocco MJ, Russ WP, Brunger AT, Engelman DM (2000) Interhelical hydrogen bonding drives strong interactions in membrane proteins. *Nat Struct Biol* 7:154–160.
52. Chill JH, Louis JM, Miller C, Bax A (2006) NMR study of the tetrameric KcsA potassium channel in detergent micelles. *Protein Sci* 15:684–698.
53. Teriete P, Franzin CM, Choi J, Marassi FM (2007) Structure of the Na,K-ATPase regulatory protein FXYD1 in micelles. *Biochemistry* 46:6774–6783.
54. Howell SC, Mesleh MF, Opella SJ (2005) NMR structure determination of a membrane protein with two transmembrane helices in micelles: MerF of the bacterial mercury detoxification system. *Biochemistry* 44:5196–5206.
55. Matthey U, Kaim G, Braun D, Wuthrich K, Dimroth P (1999) NMR studies of subunit c of the ATP synthase from Propionigenium modestum in dodecylsulphate micelles. *Eur J Biochem* 261:459–467.
56. Li X, Greenwald I (1996) Membrane topology of the C. elegans SEL-12 presenilin. *Neuron* 17:1015–1021.
57. Feng L, et al. (2007) Structure of a site-2 protease family intramembrane metalloprotease. *Science* 318:1608–1612.
58. Wang Y, Zhang Y, Ha Y (2006) Crystal structure of a rhomboid family intramembrane protease. *Nature* 444:179–180.
59. Kutzner C, et al. (2007) Speeding up parallel GROMACS on high-latency networks. *J Comput Chem* 28:2075–2084.
60. Van Der Spoel D, et al. (2005) GROMACS: Fast, flexible, and free. *J Comput Chem* 26:1701–1718.
61. Koradi R, Billeter M, Wuthrich K (1996) MOLMOL: A program for display and analysis of macromolecular structures. *J Mol Graphics* 14:51–55 29–32.